TRANSIENT COARSENING BEHAVIOUR IN THE CAHN-HILLIARD MODEL

HARALD GARCKE, BARBARA NIETHAMMER, MARTIN RUMPF, AND ULRICH WEIKARD

ABSTRACT. We study two–dimensional coarsening by simulations for the Cahn–Hilliard model. A scale invariance of the sharp interface limit of this model suggests that the characteristic length scale grows proportional to $t^{1/3}$, respectively the energy density decreases as $t^{-1/3}$. We compare the coarsening dynamics for different choices of data for different volume fractions. We observe that, depending on the specific data, the coarsening process can over a large time window be much slower than expected by dimensional analysis.

1. INTRODUCTION

The kinetics of phase separation in a binary alloy after quenching are characterized by three stages. Since for low temperatures the initially homogeneous state is unstable, first, domains of a new phase nucleate and grow rapidly in a second stage. Then, two phases have formed and are separated by interfacial layers which are much thinner than the typical diameter of the domains. In the last stage of the phase separation the system is driven by the reduction of the surface energy of these interfacial layers, which leads to an increase of the typical length scales in the system, a phenomenon known as coarsening.

A particular regime of interest is the one of an off–critical mixture where the volume fraction of one phase is small. Then this phase emerges as many small disconnected almost spherical

1991 *Mathematics Subject Classification.* 35K35, 35K55, 65L50, 65M12, 65M15, 65M60, 82B26.
Key words and phrases. Cahn-Hilliard equation, fourth order parabolic equation, finite element approximation,second order time discretization.

particles. Subsequently, larger particles grow at the expense of the smaller ones which shrink and disappear, a form of competitive growth which is also called Ostwald ripening.

Phase separation in a binary alloy is well–described by the Cahn–Hilliard equation which describes the state of by the relative concentration difference $\rho = \beta(2\frac{\rho_A}{\rho_A+\rho_B} - 1)$, where ρ_A and ρ_B are the concentrations of the two components, and $\beta \in (0, 1]$ is a parameter. The corresponding Ginzburg–Landau free energy E is defined to be

$$E(\rho) := \int_\Omega \left\{ \Psi(\rho) + \frac{\gamma}{2}|\nabla\rho|^2 \right\}, \tag{1.1}$$

where Ω is a bounded domain and γ a positive parameter. The first term in the free energy, $\Psi(\rho)$, is the chemical energy density and typically has a double well form. In this paper we take

$$\Psi(\rho) = \frac{1}{4}\big(\rho^2 - \beta^2\big)^2. \tag{1.2}$$

We note that the system is locally in one of the two phases if the value of ρ is close to one of the two minima $\pm\beta$ of Ψ.

The second term in the energy penalizes gradients with the effect that the total amount of transition zones is accounted for in the energy.

Now, the diffusion equation for the concentration ρ is given by

$$\frac{\partial\rho}{\partial t} = \Delta w \tag{1.3}$$

on $\mathbb{R}^+ \times \Omega$. In the equation above we denote by w the local chemical potential difference which is given as the variational derivative $\frac{\delta E}{\delta \rho}$ of E with respect to ρ. Thus, we obtain

$$w = -\gamma\Delta\rho + \Psi'(\rho). \tag{1.4}$$

The system has to be supplemented with boundary and initial conditions. Here we request $\partial_\nu w = \partial_\nu \rho = 0$, where ν is the outer normal on $\partial\Omega$, and $\rho(0,\cdot) = \rho_0(\cdot)$ for some initial concentration distribution ρ_0. Roughly speaking the model assumes diffusion of the species in such a way that the energy functional 1.1 is minimized as quickly as possible.

As the boundary conditions prohibit any mass flux over the boundary mass is conserved and in view of the minimization assumption it comes as no surprise that the Ginzburg–Landau free energy is a Lyapunov functional, i.e. decaying in time. Written formally we have

$$\frac{d}{dt}\int_\Omega \rho(x,t)dx = 0 \qquad \text{and} \qquad \frac{d}{dt}E\left(\rho(t)\right) \leq 0. \tag{1.5}$$

We recall that in the last stage of the evolution the system is driven by the energy of the interfaces between domains. In this regime the Cahn–Hilliard equation is well approximated by its sharp–interface limit, the so–called Mullins–Sekerka model [12, 1], which reduces the total surface area of the interface between the phases, while it keeps the volume fraction of each phase constant. Both models can be interpreted as a gradient flow of an energy, the energy is E for the Cahn–Hilliard model and the surface area in the Mullins–Sekerka model. This also reflects the fact, that for large times the energy E is dominated by the surface energy. For the corresponding stationary problem the connection between the energies has been made precise in [9].

A quantity of interest is the coarsening rate of a system, which is often measured by the growth rate of a characteristic length scale. On the level of the Mullins–Sekerka description, typical length scales are domain diameters, or in asymmetric mixtures the mean particle size. These quantities are not so well defined within the Cahn–Hilliard model. However,

we are interested in the time regime when the energy is approximately given by the interfacial area between the phases and thus the energy density has dimension $(\text{length})^{-1}$. It is therefore also natural to consider the rate of change of the energy density as a measure for the coarsening rate.

Due to an invariance of the Mullins–Sekerka model under the scaling $x \to \lambda x$, $t \to \lambda^3 t$, one expects that the characteristic length scale grows as $t^{1/3}$, which is also observed in many experiments (cf. e.g. [5] and the references in [15]). Since the volume fraction of each phase is preserved it follows that the energy density is expected to decrease as $t^{-1/3}$.

Recently, a first rigorous result concerning the coarsening rate within the Cahn–Hilliard model has been obtained in [6]. Upper bounds on the coarsening rate have been derived, by showing that in an average sense, the energy decreases at most as $t^{-1/3}$. Lower bounds have not yet been derived rigorously and can also not be expected within a deterministic framework, since there are non-generic configurations, for example configurations with no curvature of the interfaces, where coarsening is very slow.

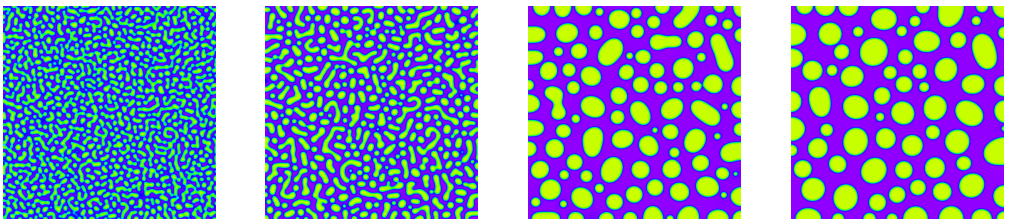

(a) $t = 0.01$ (b) $t = 0.05$ (c) $t = 1.5$ (d) $t = 3$

FIGURE 1. Evolution starting from a perturbation of a uniform state

The purpose of this note is to report on results of numerical simulations for the Cahn–Hilliard model which might further elucidate the transient behavior of a coarsening system

and its dependence on the data. In fact, when we first investigated the decrease of the energy (since our simulations are for a finite domain, we consider in the following just the total energy) for data which are perturbations of a uniform state (cf. Figures 1 and 2), we observed to our surprise that after spinodal decomposition the system settles for a "wrong" smaller exponent for quite long times, before finally the energy decreases faster. We then investigated the coarsening rates for several type of data (perturbed homogeneous states, particle seeds, set particles) for different volume fractions. We obtain a very sensitive dependence of the coarsening rate on the type of data, observing transient exponents ranging from $-1/6$ to $-1/3$. The details of the results are presented below in Section 4 after a review of the discretization and implementation of the problem in Section 2.

Let us conclude this introduction with a few remarks on the case of on an off–critical mixture with asymmetric volume fraction. In the off–critical regime, the classical mean–field theory by Lifshitz, Slyozov and Wagner [8, 16] (LSW) reduces in three dimensions the Mullins–Sekerka model to a nonlocal transport equation for the size distribution of the particles, which inherits the scale invariance $l \sim t^{1/3}$, l being the typical radius of a particle. Moreover, there are self–similar solutions, reflecting the conjecture that phase separation occurs in a statistically self–similar manner – at least for generic data. A similar theory can be developed for two–dimensional coarsening, as has been argued in

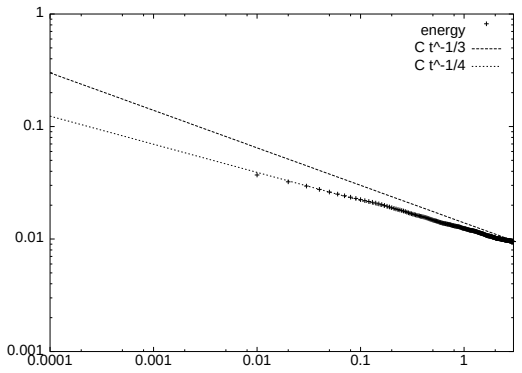

FIGURE 2. Graph of the energy (double logarithmic scale),

[13] and derived in a mathematically rigorous manner in [11]. More precisely, the analogue of the LSW–model is recovered with a scaling factor, which implies that the typical length scale grows proportional to $(t/\ln \phi^{-1/2})^{1/3}$, where ϕ denotes the volume fraction of the minority phase. This factor indicates, that – in particular in the off–critical case – the approach to the $t^{1/3}$–law might be slow in two dimensions. This is also seen in the simulations in [13], which show for the off–critical case a power law for the typical length scale with exponent $\sim .29$ instead of $1/3$.

2. Discretization

In what follows we briefly discuss the discretization and implementation of the evolution problem. For this purpose a finite element discretization in space and some discrete scheme in time are considered. We consider an appropriate continuous variational formulation for the Cahn-Hilliard equation, given by

$$(\partial_t \rho, \theta) + (\nabla w, \nabla \theta) = 0,$$

$$(w, \xi) = \left(\Psi'(\rho), \xi\right) + \gamma \left(\nabla \rho, \nabla \xi\right),$$

which has to hold for all $\theta, \xi \in C^\infty(\bar{\Omega})$, where $(\cdot, \cdot)$ denotes the L^2-product on the domain Ω. For a finite element implementation we now replace the continuous solution and test functions in this formulation by discrete approximations in some finite element space. Here we have restricted ourselves to finite elements on regular adaptive grids in 2D generated by recursive subdivision of some macro elements. We consider triangular Courant elements as well as bilinear finite elements on quadratic grids. We will denote the finite element space for the approximation of ρ and w on Ω with V^h . Numerical integration of the L^2-products

is based on the lumped masses product $(\cdot,\cdot)_h$ [14]. Furthermore we consider a center of mass quadrature rule for the bilinear form $(\nabla\cdot,\nabla\cdot)$.

For the discretization in time we have taken into account two possibilities: a first order implicit Euler scheme and a second order θ–splitting scheme (see Bristeau et al. [2] and Müller Urbaniak [10]). Both are known to be strongly A–stable. While we can prove the energy decay property for the implicit Euler scheme, we use the θ–splitting for practical computations as it allows larger time steps.

In the case of the implicit Euler scheme the time derivative is discretized by $\partial_t\rho((n+1)\tau) \approx \frac{\rho^h_{n+1}-\rho^h_n}{\tau}$ where τ is the selected time step and ρ^h_n an approximation of $\rho(n\tau)$. A brief introduction to the more complicated θ–splitting can be found in [4].

Finally, we can derive a fully discrete scheme. For the "hat shaped" multi linear basis functions ϕ_i we define by

$$M_h := \left((\phi_i,\phi_j)_h\right)_{ij},$$

$$L_h := \left((\nabla\phi_i,\nabla\phi_j)\right)_{ij}$$

the diagonal lumped mass and the standard stiffness matrix. These global matrices M_h and L_h are assembled in a grid traversal collecting the contributions on all local grid elements as it is standard in finite element programming [3].

If we indicate by a bar coefficient vectors corresponding to finite element functions in the basis $\{\phi_i\}_i$, we obtain the backward Euler discretization

$$M_h\bar\rho^h_{n+1} + \tau L_h\left(\bar\Psi'(\bar\rho^h_{n+1}) + \gamma M_h^{-1}L_h\bar\rho^h_{n+1}\right) = M_h\bar\rho^h_n$$

with $\rho_0^h = \mathcal{I}_h \rho_0$, where $\mathcal{I}_h$ is the interpolation on grid M_h. By obvious notation $\bar{\Psi}'(\cdot) := (\Psi'(\cdot))_i$ is the vector of nodal wise derivatives of Ψ.

In each step of the discrete evolution we have to solve this system of nonlinear equations. In order to do this we apply some Newton scheme which typically converges in a few steps if we consider moderate time steps and pick up the old solution at the old time step as the initial guess for the Newton iteration.

The efficiency of our approach is further increased by an adaptive grid refinement and coarsening strategy. Here, we used a heuristic strategy which refines in interfacial regions and coarsens in the pure phases.

In the case of the implicit Euler scheme, it is possible to prove discrete counterparts of the mass conservation and energy decay properties. I. e.

$$\int_\Omega \rho_n^h \, dx = \int_\Omega \mathcal{I}_h \rho_0 \, dx \tag{2.1}$$

and

$$E_h(\rho_n^h) := \int_\Omega \left\{ \mathcal{I}_h \Psi(\rho_n^h) + \frac{\gamma}{2} \nabla \rho_n^h \cdot \nabla \rho_n^h \right\} dx \tag{2.2}$$

is non increasing in time (discrete Lyapunov property).

3. Tests of the implementation

As the results stated in this paper are somewhat surprising and the discretization error is potentially very large (stability estimates for the Cahn-Hilliard equation usually deteriorate like $e^{\frac{1}{\gamma}}$) we performed several tests. First, in order to exclude coding errors we used two different implementations: one using linear finite elements on a triangular grid, the other one using bilinear elements on a quadratic grid. Both implementations showed exactly the

same behaviour concerning time scales and speed of the evolution. Second we established via numerical experiments that the grid sizes and time step sizes we used for the actual calculations were in an asymptotic regime. Finally we computed the evolution for several problems which were just scaled versions of each other. We then checked if the algorithm showed the appropriate time scaling in the solution, which it did.

4. Numerical Results

In the exposition of our numerical results we focus on the evolution of the total energy. Other quantities, which would equivalently characterize the coarsening process, are for example the average particle size or the average interparticle distance. However, within the Cahn–Hilliard model, we would need a necessarily somewhat arbitrary criterion of what a particle and its size are. The application of such criteria proves difficult in the case when particles are vanishing or merging. Once the interfacial regime has emerged, the total energy is proportional to the surface area of the interface, i.e. to the sum of the perimeters of all particles. As the total volume of all particles is constant, it immediately follows that the total energy evolves proportional to the inverse of the average radius. Hence, since we expect the average particle size to increase as $t^{1/3}$, we expect the total energy to decrease as $t^{-1/3}$. For all calculations the domain has been the square $[0,3] \times [0,3]$ and the parameter of the energy have been $\gamma = 10^{-5}$ and $\beta = 0.4$ while we chose the time step size to be $5 \cdot 10^{-4}$.

4.1. **Evolutions starting from a perturbation of a uniform state.** Let us first consider the evolution already shown in Figures 1 and 2. After long times ($t > 7$) the energy decay differs from the behaviour at earlier times. In contrast to the decay depicted in Figure 2

we observe a graph like in Figure 3. Here we see time intervals where the energy goes according to $E \approx Ct^{-\frac{1}{3}}$ which are intersected by short periods, when the energy decays faster. In these short periods one sees particles vanishing, whereas between these steeper declines particles are just growing and shrinking with the number of particles constant. In

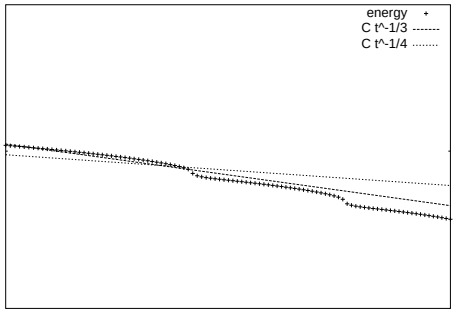

FIGURE 3. Graph of the energy in the late stage of the evolution

the calculation discussed so far the ratio of the volume fraction of the two phases has been $60 : 40$. We observed a dependence of the transition time to the expected growth law on the volume fraction of the phases. The transition time is drastically shorter in the case of equal volume fractions. Figure 5 shows such an evolution and the corresponding energy graph is depicted in Figure 4. Other computations confirmed that the transient growth exponent depends smoothly on the mass fractions of the initial data.

4.2. **The evolution starting with set particles.** The same transient behaviour can be observed in the case of initial data in which a given number of randomly chosen particles are set in a uniform state. In Figure 6 a calculation on a $[0, 3] \times [0, 3]$ square is shown. Figure 7 shows the corresponding energy graph. Again it takes considerable time until the system settles to the expected growth law.

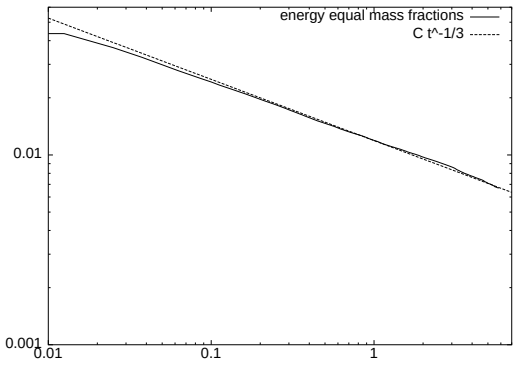

FIGURE 4. Graph of the energy with equal mass fractions

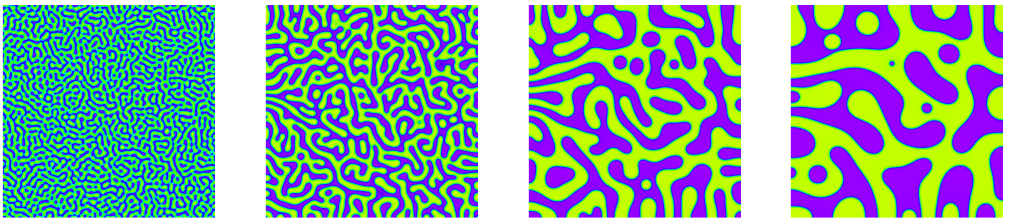

(a) $t = 0.025$ (b) $t = 0.125$ (c) $t = 1.25$ (d) $t = 4.875$

FIGURE 5. Evolution with equal mass fractions

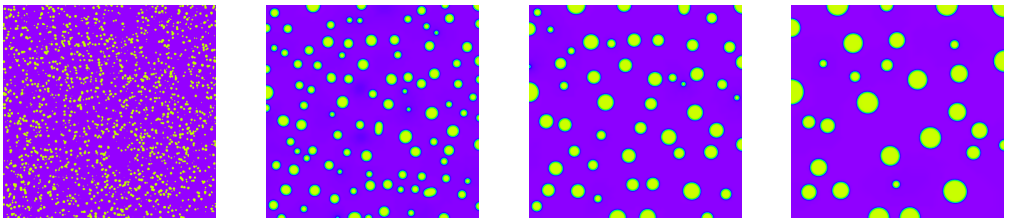

(a) $t = 0.0125$ (b) $t = 0.25$ (c) $t = 2.25$ (d) $t = 6.7$

FIGURE 6. Evolution with set particles

4.3. **The evolution starting with particle seeds.** In Figure 8 an evolutions is shown, where the initial value has been a uniform mixture in which a given number of randomly chosen

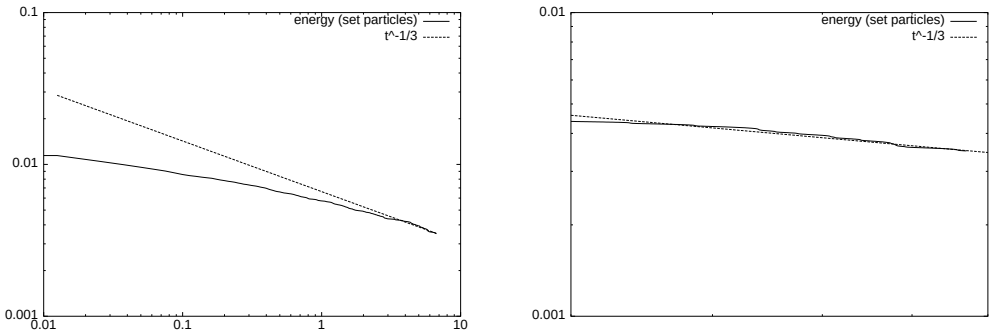

(a) Graph of the energy

(b) Late stage of the evolution for $t = 3$ to 7

FIGURE 7. Evolution with set particles

particle seeds are set. A particle seed is a ball shaped area, where the concentration is slightly above the value of the uniform mixture but in neither of the two minima of the double well potential. The two graphs Figure 8(e) and 8(f) show the evolution of the energy and as a reference line the function $ct^{-\frac{1}{3}}$.

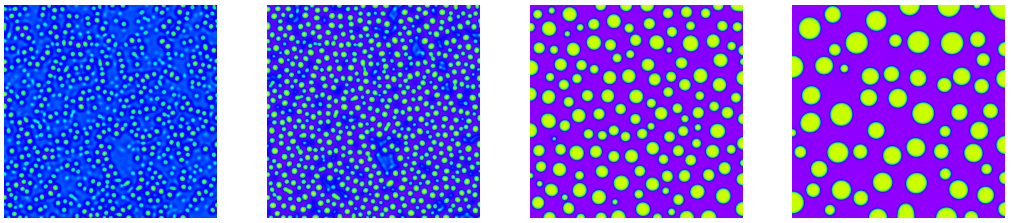

(a) $t = 0.025$ (b) $t = 0.0375$ (c) $t = 1.25$ (d) $t = 5.5$

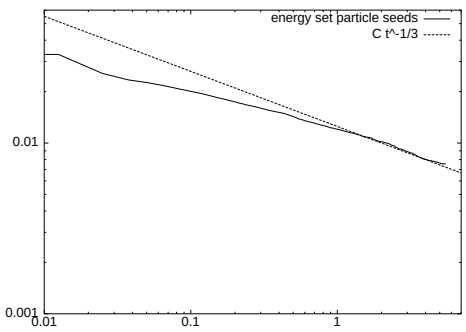

(e) evolution of the energy

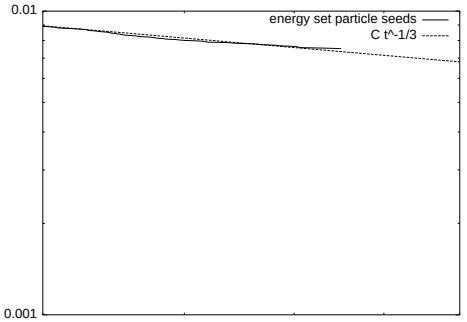

(f) $t \in [3, 7]$

FIGURE 8. Initial value: particle seeds

REFERENCES

[1] N. Alikakos, P. Bates and X. Chen, Convergence of the Cahn-Hilliard equation to the Hele–Shaw model, Arch. Rat. Mech. Anal., 128 (1994), pp. 165–205.

[2] M.O. Bristeau, R. Glowinski and J. Periaux, Numerical Methods for the Navier-Stokes equations: Applications to the simulation of compressible and incompressible viscous flows, Computer Physics Report, Research Report UH/MD-4, University of Houston, 1987

[3] P.G. Ciarlet, The Finite Element Method for Elliptic Problems, North-Holland, 1978

[4] H. Garcke, M. Rumpf and U. Weikard, The Cahn-Hilliard equation with elasticity: Finite element approximation and qualitative studies, Interfaces and Free Boundaries **3** (2001), 101–118

[5] S.C. Hardy and P.W. Voorhees, Ostwald ripening in a system with a high volume fraction of coarsening phase , Met. Trans. A **19** A (1988), 2713-2721

[6] R. V. Kohn and F. Otto, Upper bounds for coarsening rates, to appear in Comm. Math. Phys.

[7] T. Küpper and N. Masbaum, Simulation of particle growth and Ostwald ripening via Cahn-Hilliard equation, Acta metall. mater. **42** No. 6 (1994), 1847–1858

[8] I.M. Lifshitz and V.V. Slyozov, The kinetics of precipitation from supersaturated solid solutions, J. Phys. Chem. Solids **19** (1961), 35-50

[9] L. Modica, The gradient theory of phase transitions and the minimal interface criterion , Arch. Rat. Mech. Anal. **98** (1987), 123-143

[10] S. Müller-Urbaniak, Eine Analyse des Zweischritt-θ-Verfahrens zur Lösung der instationären Navier-Stokes-Gleichungen, Preprint des SFB 359, No. 94 - 01, 1994

[11] B. Niethammer and F. Otto, Domain coarsening in thin films , Comm. Pure Appl. Math. **54** (2001), 361-384

[12] R. Pego, Front migration in the nonlinear Cahn-Hilliard equation, Proc. Roy. Soc. London A, 422 (1989), 261–278.

[13] T. M. Rogers and R. C. Desai, Numerical study of late–stage coarsening for off–critical quenches in the Cahn–Hilliard equation of phase separation , Phys. Rev. B **39** 16 (1989), 11956-11964

[14] V. Thomée, Galerkin Finite Element Methods for Parabolic Problems, Springer, 1984

[15] P. W. Voorhees, The theory of Ostwald ripening, J. Stat. Phys. **38** (1985), 231-252

[16] C. Wagner, Theorie der Alterung von Niederschlägen durch Umlösen, Z. Elektrochem., 65 (1961), 581-594.

HARALD GARCKE,

NATURWISSENSCHAFTLICHE FAKULTÄT I - MATHEMATIK,

UNIVERSITÄT REGENSBURG

93040 REGENSBURG, GERMANY

harald.garcke@mathematik.uni-regensburg.de

BARBARA NIETHAMMER,

INSTITUT FÜR ANGEWANDTE MATHEMATIK, UNIVERSITÄT BONN,

WEGELERSTR. 6, 53115 BONN, GERMANY,

barbara@iam.uni-bonn.de

MARTIN RUMPF, ULRICH WEIKARD

INSTITUT FÜR MATHEMATIK

FAKULTÄT 4, NATURWISSENSCHAFTEN

GERHARD-MERCATOR-UNIVERSITÄT DUISBURG

LOTHARSTR. 65

47048 DUISBURG

rumpf,weikard@math.uni-duisburg.de